JOURNAL OF BIOMEDICAL OPTICS 3(1), 45–54 (JANUARY 1998)

SIGNAL AND RESOLUTION ENHANCEMENTS IN DUAL BEAM OPTICAL COHERENCE TOMOGRAPHY OF THE HUMAN EYE

Angela Baumgartner, Christoph K. Hitzenberger, Harald Sattmann, Wolfgang Drexler, and Adolf F. Fercher

Institute of Medical Physics, University of Vienna, Währinger Straße 13, A-1090 Vienna, Austria

(Paper JBO/IB-011 received Aug. 21, 1997; revised manuscript received Nov. 11, 1997; accepted for publication Nov. 12, 1997.)

ABSTRACT

In the past 10 years, a dual beam version of partial coherence interferometry has been developed for measuring intraocular distances *in vivo* with a precision on the order of 0.3 to 3 μm. Two improvements of this technology are described. A special diffractive optical element allows matching of the wavefronts of the divergent beam reflected at the cornea and the parallel beam reflected at the retina and collimated by the optic system of the eye. In this way, the power of the light oscillations of the interfering beams incident on the photodetector is increased and the signal-to-noise ratio of *in vivo* measurements to the human retina is improved by 20 to 25 dB. By using a synthesized light source consisting of two spectrally displaced superluminescent diodes with an effective bandwidth of 50 nm, and by compensating for the dispersive effects of the ocular media, it was possible to record the first optical coherence tomogram of the retina of a human eye *in vivo* with an axial resolution of ~6 to 7 μm. This is a twofold improvement over the current technology.
 [S1083-3668(98)01601-3]

Keywords partial coherence interferometry; optical coherence tomography; resolution; dispersion; diffractive optics; human eye; retina.

1 INTRODUCTION

Tomographic images of retinal structures *in vivo* as well as the quantitative and precise measurement of the thickness of various fundus layers at arbitrary reproducible measurement positions are clinically essential in modern ophthalmology for diagnosis, monitoring, and therapy control of ocular diseases. Glaucoma, macular degeneration, edema, and many other optic neuropathies are accompanied by alterations of the retinal thickness or the retinal nerve fiber layer thickness.

Retinal imaging of high lateral resolution can be obtained by scanning laser ophthalmoscopy, and with improved depth resolution, by confocal scanning laser tomography.[1–4] However, the axial resolution of these methods is limited by the pupil diameter and ocular aberrations. A very fast and precise method for measuring the thickness of the retinal nerve fiber layer is scanning laser polarimetry, a technique that measures the retardation of laser light passing through the birefringent retinal nerve fiber layer.[5,6]

Retinal thickness can be measured by ultrasonography using high frequencies[7,8] and by a noninvasive optical technique employing an extension of slit-lamp biomicroscopy.[9,10] However, both methods are limited in their longitudinal resolution. Another drawback of the ultrasound technique is the mechanical contact needed between the eye and the instrument.

In the past 10 years a new interferometric technique for length measurement, partial coherence interferometry (PCI), has been developed. The first applications of this technique to measure the axial length in human eyes *in vivo* were reported by Fercher and Roth[11] and Fercher, Mengedoht, and Werner.[12] Since a classic interferometric setup is extremely sensitive to longitudinal motion of an object, a special dual beam interferometry technique was used to eliminate the influence of longitudinal eye motion. An electronic fringe detection system using the Doppler principle was introduced to reduce the measuring time.[13,14] This method of dual-beam PCI enables high-precision biometry of the human eye *in vivo*, measuring corneal thickness,[14,15] anterior chamber depth,[15,16] lens thickness,[15,16] the axial eye length,[13] the thickness of the retina,[13,17] and various fundus layers very accurately at arbitrary positions of the human eye fundus. This technique has been further extended to optical coherence tomography (OCT), a new imaging modality

Address all correspondence to Angela Baumgartner. Tel: 431 40480333; Fax: 431 4024030; E-mail: angela.baumgartner@univie.ac.at

1083-3668/98/$10.00 © 1998 SPIE

capable of obtaining two-dimensional sections of the human retina.[18–21] For a recent overview of OCT, see Ref. 22. Recent developments in OCT are concerned with improving axial resolution[23] and with the development of an alternative OCT scheme that enables the recording of en face images.[24,25]

The measurement of intraocular distances by the dual beam PCI technique is based on the detection of interference fringes caused by light beams reflected at the various intraocular interfaces whose distances are to be measured. In order to be detected, the spacing of the interference fringes must be wider than the effective diameter of the photodetector. Since the positions of the intraocular interfaces are measured with respect to the anterior corneal surface as the reference surface, a concentric ring-shaped interference fringe system is formed due to the dual beam interference of the divergent beam reflected at the anterior corneal surface and the almost parallel beam reflected at the retina and refracted by the lens and the cornea.[11] Owing to the wavefront mismatch of the two interfering beams, the corresponding interference fringes are narrow and a photodetector with a small area (50 μm diameter) has to be used. This limits the intensity incident on the photodetector and hence the signal-to-noise ratio (S/N) obtainable with the motion-insensitive dual beam PCI technique. In order to improve the S/N, the PCI technique has now been further extended by using a diffractive optical element that compensates for this wavefront mismatch.[26,27] By the use of this element, both of the interfering beams reflected at the cornea and the retina will be collimated when they recombine at the photodetector so that all the optical power reflected by the eye may be collected. In this way, a significant improvement of the signal-to-noise ratio is achieved. This paper demonstrates the signal improvement achieved in this way and presents the first retinal *in vivo* tomograms recorded in a human eye with this technique.

In OCT, longitudinal resolution depends on the spectral bandwidth of the light source used and on the dispersion of the media to be measured. In nondispersive media, the resolution is approximately equal to the coherence length of the light used, which is inversely proportional to the width of the emission spectrum.[28] Hence a broad emission spectrum yields a short coherence length and consequently a good resolution. With currently used superluminescent diodes (SLDs), resolutions on the order of 10 to 15 μm are achieved. By using a broadband Ti:Al_2O_3 source, a resolution of a few microns was recently demonstrated in biological tissue with a total thickness of a few hundred microns.[23] However, if the tissue under investigation is dispersive, the coherence envelope of the signal broadens due to the different velocities of the various wavelengths of the broad emission spectrum in the dispersive medium, leading to a decrease in resolution and interference fringe contrast. We have recently demonstrated that this effect becomes dominant if measurements through the dispersive media of the eye to the retina are performed with source bandwidths larger than about 25 nm.[29,30]

In order to achieve optimum resolution of OCT by applying a light source with a broad emission spectrum, the dispersion of the object to be measured (in this case the ocular media) has to be compensated for. This can be achieved by placing a dispersive element in the reference arm of the Michelson interferometer that causes the same group dispersive effect as the ocular media.[30] It is the second purpose of this paper to demonstrate the improvement in resolution that is obtained by compensating for the object dispersion and using a light source of 50 nm bandwidth consisting of two spectrally displaced SLDs. Furthermore, we present the first OCT image recorded with this technique in a human eye *in vivo* with an axial geometrical resolution of about 6 μm.

2 METHODS

2.1 DUAL BEAM PARTIAL COHERENCE INTERFEROMETER

The theory and experimental details of measuring intraocular distances by dual beam PCI was described in previous papers.[13,14] Therefore, only a brief summary is presented here.

As depicted in Figure 1, a superluminescent diode emits a light beam of high spatial coherence but short coherence length l_c which illuminates an external Michelson interferometer. The interferometer splits the beam into two coaxial components that have a phase difference corresponding to twice the interferometer arm length difference d. This dual beam illuminates the eye, where each subcomponent is reflected at the various intraocular interfaces separating regions of different refractive indices. If the difference in arm length of the Michelson interferometer equals (within l_c) one of the intraocular distances to be measured, the beams reflected at the respective intraocular interfaces will interfere. During the measurement, one of the mirrors of the Michelson interferometer is moved by a stepper motor with a constant speed ν, which causes a Doppler shift of the light frequency of the corresponding beam. In the case of a coincident path length, the intensity of the corresponding interference pattern is modulated by the Doppler frequency $f_D = 2\nu/\lambda$. The superimposed reflected beams are then focused onto the photodetector, amplified, and filtered by a bandpass filter that transmits only signals with f_D. The envelope of this signal is recorded as a function of the interferometer's arm length difference d with a personal computer. The signal curves recorded in this way are called PCI scans, or optical A-scans, and contain characteristic

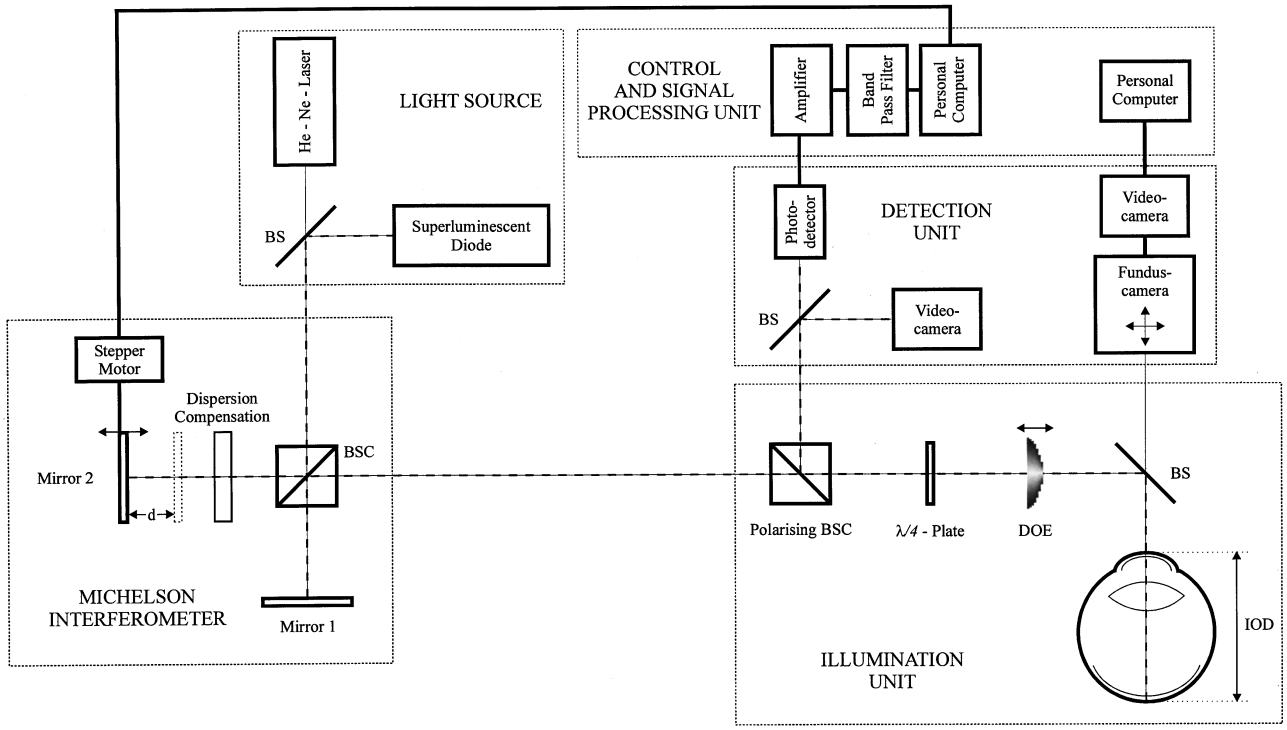

Fig. 1 Schematic of the improved dispersion compensated partial coherence interferometer with the modified illumination unit employing a diffractive optical element and the implementation of a fundus camera. BSC, beamsplitter cube; BS, beamsplitter; IOD, intraocular distance.

signal peaks. From the positions of these peaks on the d axis, the respective optical intraocular distances (IOD) can be determined: IOD$=d\pm l_c$. Using a cursor readout to determine the signal peak position in the PCI scan provides a precision even better than l_c. To convert the optical intraocular distance into the appropriate geometrical distance, it must be divided by the group refractive index n_g of the respective medium.[13]

Simultaneous with the optical A-scans of the PCI system, the eye under investigation can be examined by a fundus camera.[27] As depicted in Figure 1, the laser light illuminates the eye via a short-wave pass beamsplitter that reflects light in the near-infrared (IR) region ($\lambda=760$ to 850 nm) and transmits the white light of the fundus camera in front of the eye ($\lambda=450$ to 650 nm). For this purpose, the pupil of the eye to be measured has to be dilated by a mydriaticum. First the eye is aligned with the incident laser beam; then the fundus camera is adjusted to its appropriate working distance in order to get the fundus image showing the position of the incident laser spot on the retina. The image of the fundus camera can be observed on-line via a visible and near-IR sensitive CCD camera that is connected to a personal computer via a frame grabber card to store the appropriate fundus images and enable the exact localization of the measurement position.

2.2 WAVEFRONT MATCHING

The major drawback of the dual beam version of partial coherence interferometry is the poor signal-to-noise ratio due to the wavefront mismatch of the two interfering beams reflected at the anterior corneal surface and the retina. If the probing beam is collimated, the light reflected at the retina will be collimated by the optical elements of the human eye (in case of emmetropic subjects) while the beam reflected at the cornea will be divergent. If the probing beam is focused at the cornea, the reflected beam from the cornea will again be collimated by the focusing lens, but the light reflected at the retina will be divergent. In either case, a concentric ring-shaped interference fringe system as depicted in Figure 2 is formed.[12] The spacing of these circular interference fringes becomes smaller at the periphery of the fringe pattern. Ideally, the photodetector should be aligned with the center of the fringe system. Because ocular motion cannot be completely avoided during *in vivo* measurements, this ideal alignment cannot be perfectly maintained. Therefore, the diameter of the photodetector has to be small enough that even in the case of slight misalignments, only a single fringe is imaged onto the detector surface. A detector diameter of $\sim 50\,\mu$m turned out to be optimal.[13] In this case, however, the total light power collected by the detector is rather low, and therefore the S/N is poor.

In order to overcome this drawback, we used a special diffractive optical element for wavefront matching.[26,27] This sort of Fresnel's zone lens is implemented in front of the eye in order to focus part of the incident laser beam on the vertex of the cornea ($f=70$ mm). The other collimated parallel

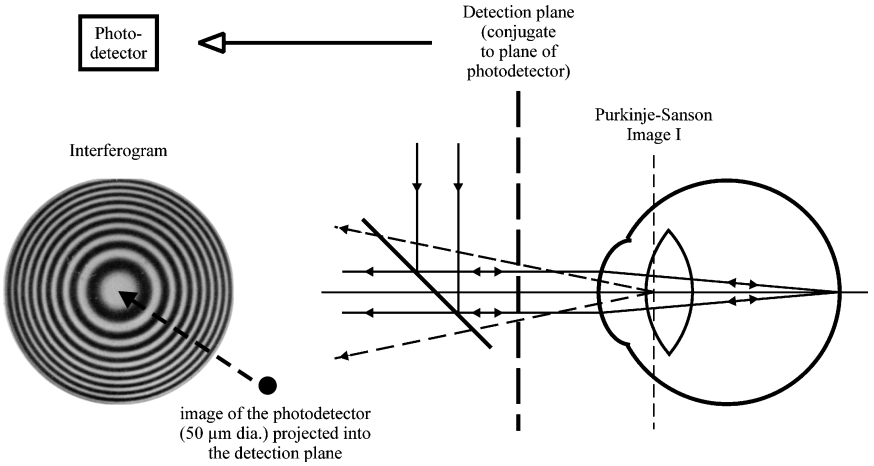

Fig. 2 Schematic of the concentric ring-shaped interference fringe system due to the dual beam interference of the divergent corneal reflection and the parallel retinal reflection. The photodetector has to be aligned approximately coaxially to the center of the interference fringe system.

part of the beam passes through uninfluenced (Figure 3). This part of the beam will be focused onto the retina (in case of emmetropic subjects) by the optical elements of the human eye.

The beams remitted from the anterior corneal surface and the retina will thereby both be converted into parallel beams when they pass again through the diffractive optical element (DOE) on their way back to the detection unit. Assuming a reflectivity of $\rho = 2\%$ of the anterior corneal surface and $\rho = 1\%$ of the retina (corresponding to data recorded with an experimental laboratory setup), the DOE has been designed to focus 40% of the intensity of the incident laser beam on the vertex of the cornea and to let 60% pass through as a collimated parallel beam. Under these circumstances, the theoretical visibility of the interference fringes should be approximately 1. Consequently, two collimated parallel beams will interfere and the light power oscillations in the corresponding interferograms will be much stronger than those of the narrow interference fringes obtained without that technique. This improves the signal-to-noise ratio considerably. The alignment of the DOE in front of the eye takes only a few seconds and is easy to perform. Once the eye under investigation is adjusted properly, the alignment is not more sensitive to movements of the eye than with the previous arrangement.

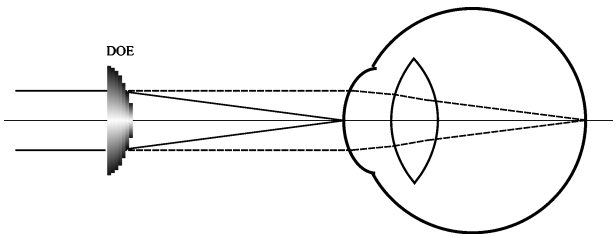

Fig. 3 Schematic of the principle of the diffractive optical element. Part of the incident laser beam will be focused on the vertex of the cornea, the other collimated parallel part of the beam will pass through uninfluenced. This part of the beam will be focused onto the retina (in case of emmetropic subjects) by the optical elements of the human eye. Both of the beams reflected at the cornea and the retina will be collimated when they pass through the DOE on their way back to the detection unit.

2.3 LIGHT SOURCE

As already mentioned, the resolution of PCI is approximately equal to the coherence length of the light source used. Assuming a Gaussian shape of the emission spectrum, the full-width at half-maximum (FWHM) round-trip coherence length l_c in a PCI system with a Michelson interferometer can be calculated[23]:

$$l_C = \frac{2\ln(2)}{\pi} \times \frac{\lambda_0^2}{\Delta\lambda}, \tag{1}$$

where λ_0 is the center wavelength of the source and $\Delta\lambda$ is its FWHM spectral width.

Within the scope of this work, two different light sources have been used: A single superluminescent diode (EG&G C86142E, EG&G Optoelectronics, Canada) with $\lambda_0 = 830$ nm and $\Delta\lambda = 26$ nm. According to Eq. (1), the coherence length $l_c = 11.7$ μm. For demonstration of high-resolution OCT, a synthesized light source generated by superimposing two superluminescent diodes (EG&G C86142E, EG&G Optoelectronics, Canada) with different center wavelengths ($\lambda_{01} = 830$ nm, $\Delta\lambda_1 = 26$ nm, $\lambda_{02} = 855$ nm, and $\Delta\lambda_2 = 25$ nm) has been used. Owing to a beat effect,[31–33] these two combined light sources have an effective spectral width of $\Delta\lambda_{\text{eff}} = 50$ nm. The coherence length of this synthesized light source $\lambda_c \approx 8$ μm.

2.4 DISPERSION COMPENSATION

If one of the beams in a PCI system travels through a dispersive medium while the other travels

through air (or if the path lengths through dispersive media differ in length), the coherence envelope of the optical A-scans broadens and the resolution decreases. If the length of a dispersive medium in one of the interferometer arms is L and the group dispersion of the medium is $dn_g/d\lambda$, the width of the coherence envelope, after double passing through the medium, can be calculated by[29,30]:

$$l_{C,m}=\left[l_C^2+\left(\frac{dn_g}{d\lambda}\times L\times\Delta\lambda\right)^2\right]^{1/2}. \quad (2)$$

The mean group dispersion of the ocular media is approximately $-1.8\times10^{-5}/\text{nm}$[34] in the near infrared. Assuming a mean axial eye length of 24 mm, the signal width, after passing through the eye media to the retina and returning, can be calculated by Eq. (2) to be $\sim$16.2 μm in the case of the single SLD with $\Delta\lambda=26$ nm and $\sim$22.5 μm in the case of a combination source with $\Delta\lambda_{\text{eff}}=50$ nm. This means that the resolution in the case of a larger source bandwidth is not improved, but degraded. In order to achieve the optimum resolution obtainable with the broadband light source, the dispersion of the ocular media has to be compensated for. This can be achieved by placing a dispersion-compensating element in the longer arm of the external Michelson interferometer (Figure 1). This element must fulfill the condition

$$L_{\text{el}}\left(\frac{dn_g}{d\lambda}\right)_{\text{el}}=L_{\text{ob}}\left(\frac{dn_g}{d\lambda}\right)_{\text{ob}}, \quad (3)$$

where the indices el and ob refer to the compensation element and the object, respectively. As a dispersion compensation element we used a plane-parallel plate of BK7 optical glass with $L_{\text{el}}=12$ mm and $(dn_g/d\lambda)_{\text{el}}\approx4\times10^{-6}$ /nm at a wavelength of $\lambda\cong840$ nm.[35] This element fulfills Eq. (3) to within a few percent and therefore compensates for most of the dispersive effects of the ocular media.[30]

2.5 TOMOGRAPHIC MEASUREMENTS

For tomographic recordings, a separate fixation light was installed in front of the eye under investigation, which encloses an adjustable vertical and horizontal angle with the measuring beam and is collimated in order to make the subject look toward infinity. This allows the rotation of the eye to be measured in order to adjust a defined arbitrary angle between the vision axis and the measuring direction. Once the eye looks at the fixation target, it is aligned with the measuring beam so that the two image points of the anterior corneal surface and the retina are centered and become confocal on the detector. For observation purposes, the detection plane is imaged onto a CCD camera where the confocal alignment can be monitored.

To obtain OCT images, several optical A-scans are recorded at different equidistant angles to the vision axis. The angle increment was 0.5 deg, corresponding to length increments of $\sim$150 μm on the retina. The intensity values of the optical A-scans are converted into pixel colors (logarithmic scale) and mounted to form a two-dimensional false color image. The pixels between the individual scanning directions are obtained by linear interpolation.

2.6 *IN VIVO* MEASUREMENTS AND LASER SAFETY

In vivo measurements were performed in healthy, volunteer subjects after full informed consent was obtained. Optical A-scans were performed over a maximum length increment of 3 mm, which takes approximately 0.4 s. Performing eight scans at most for each measurement direction for further improvement of S/N by averaging, the maximum time of continuous illumination of one point on the retina is about 4 to 5 s. During this time, the eye is illuminated with a laser light power of approximately 200 μW or an intensity of 520 $\mu\text{W}/\text{cm}^2$ (averaged over a 7-mm aperture). This is permitted for 25 min for a wavelength of $\lambda=830$ nm in the case of intrabeam viewing.[36] Since only 60% of the incident light power is focused at the retina, the laser safety limit can be easily met.

3 RESULTS

3.1 IMPROVEMENT OF THE SIGNAL-TO-NOISE RATIO

In order to quantify the improvement in the signal-to-noise ratio from the use of the diffractive optical element, measurements were taken on a model eye that consisted of a biconvex lens ($f=30$ mm) and a mirror (simulating the fundus of the eye) at a distance approximately 30 mm from the lens. Various neutral density filters were put between the lens and the mirror in order to reduce the intensity reflected at the mirror with respect to that reflected at the anterior lens surface. The model eye fundus measurements were performed under the same experimental settings as was the case for *in vivo* measurements. A single SLD ($\lambda_0=830$ nm, $\Delta\lambda=26$ nm) was used to illuminate the model eye with a light power of approximately 200 μW. According to the model eye measurement, the application of the DOE increased the signal-to-noise ratio by about 40 to 45 dB compared with previous measurements without that element.

In vivo measurements have been performed at various positions along the papillomacular axis of the fundus, within the angular range of 5 deg temporal to 20 deg nasal. As an example, Figure 4 shows an optical A-scan obtained in a healthy human eye *in vivo* at an angle of 4.5 deg nasal to the vision axis. The signal intensity (ordinate), which is proportional to the interference fringe contrast, is plotted as a function of the interferometer's arm

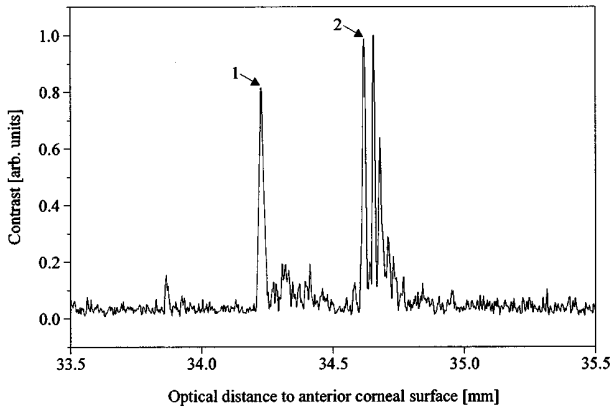

Fig. 4 Optical A-scan recorded in a human eye *in vivo* at an angle of 4.5 deg nasal to the vision axis using the diffractive optical element. The signal intensity, which is proportional to the interference fringe contrast, is plotted as a function of the interferometer's arm length difference d. Several peaks from different retinal microstructural layers can be differentiated very clearly from noise. Peak 1 probably arises from the inner limiting membrane, peak 2 probably originates from the retinal pigment epithelium. The distance between peaks 1 and 2 corresponds to the optical thickness of the retina (391 μm). The peaks behind peak 2 are probably caused by choroidal structures.

length difference d (abscissa). In this case, d was scanned over a range of 2 mm, from 33.5 to 35.5 mm. Several peaks from different retinal microstructural layers can be differentiated very clearly from noise. Peak 1 probably arises from the inner limiting membrane, the closest layer to the vitreous. Peak 2 originates probably from the retinal pigment epithelium. The distance between peaks 1 and 2 corresponds to the optical thickness of the retina (391 μm). The peaks behind peak 2 are probably caused by choroidal structures.

To demonstrate the improvement in the signal-to-noise ratio achieved by the DOE, Figure 5 shows an optical A-scan carried out with the previous version of the PCI without the application of the diffractive optical element. This measurement was performed at a horizontal angle of 10 deg nasal. It can be seen

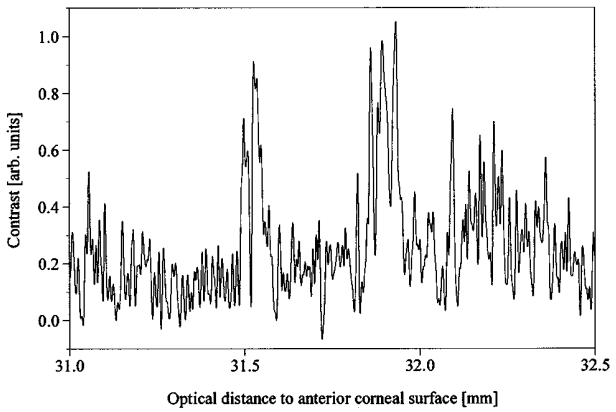

Fig. 5 Optical A-scan recorded in a human eye *in vivo* without using the DOE at an angle of 10 deg nasal to the vision axis.

clearly in a comparison with Figure 4 that the signal-to-noise ratio is improved significantly by the DOE (on the order of 20 to 25 dB). In Figure 4 the signals from the different fundus layers can be clearly differentiated from noise although the stepper motor and the measuring electronics of the PCI system using the DOE are not yet optimized.

3.2 RESOLUTION IMPROVEMENT IN OCT IMAGING

To demonstrate the improvement in axial resolution, we recorded three OCT tomograms of the same area of the same human eye *in vivo* (Figure 6—color plate). A horizontal section through the fovea centralis, from 5 deg temporal to 5 deg nasal is shown. Figure 6(a) was recorded with a single SLD ($\Delta\lambda = 26$ nm) without dispersion compensation. Figure 6(b) was recorded with the same light source, but with dispersion compensation, and Figure 6(c) was recorded with the combination source ($\Delta\lambda_{\text{eff}} = 50$ nm) and with dispersion compensation. Several microstructural layers can be observed in these figures: the inner limiting membrane, the foveal depression, the nearly transparent retina, and highly reflective layers at the posterior side of the retina. The first of these layers is probably the inner limiting membrane (ILM) that separates the retinal structures from the vitreous. In Figure 6(a), two different layers approximately 390 μm behind the ILM can be observed; however, these partly overlap (the color coding on a logarithmic scale tends to reduce the visibility of closely related details). The axial resolution in this figure is $\sim$16.5 μm optical distance (measured from optical A-scans, see Figure 7) or 12 μm geometrical distance, assuming a group refractive index of $\sim$1.4 for the retina. In Figure 6(b), the resolution improved to $\sim$13.5 μm optical distance ($\sim$9.5 μm geometrical distance) because of dispersion compensation. The three layers observed behind the ILM are much better separated. Finally, the best resolution is obtained with the broadband synthesized light source with dispersion compensation [Figure 6(c)]. The resolution, as measured from optical A-scans, is $\sim$9 to 10 μm optical distance or $\sim$6 to 7 μm geometrical distance. The three layers posterior to the retina are now imaged as three narrow, well-separated bands.

To elucidate the improvement in resolution, we have taken two individual optical A-scans from the data sets used to synthesize the tomograms of Figures 6(a) and 6(c) and superimposed them. The result is shown in Figure 7. These A-scans correspond to a measuring angle of 1.5 deg nasal to the vision axis and cover an optical distance of $\sim$100 μm. The dashed line shows the signal recorded with the single SLD without dispersion compensation; the solid line is the signal obtained with the combination source and with dispersion compensation. The improvement of the resolution is obvious: the

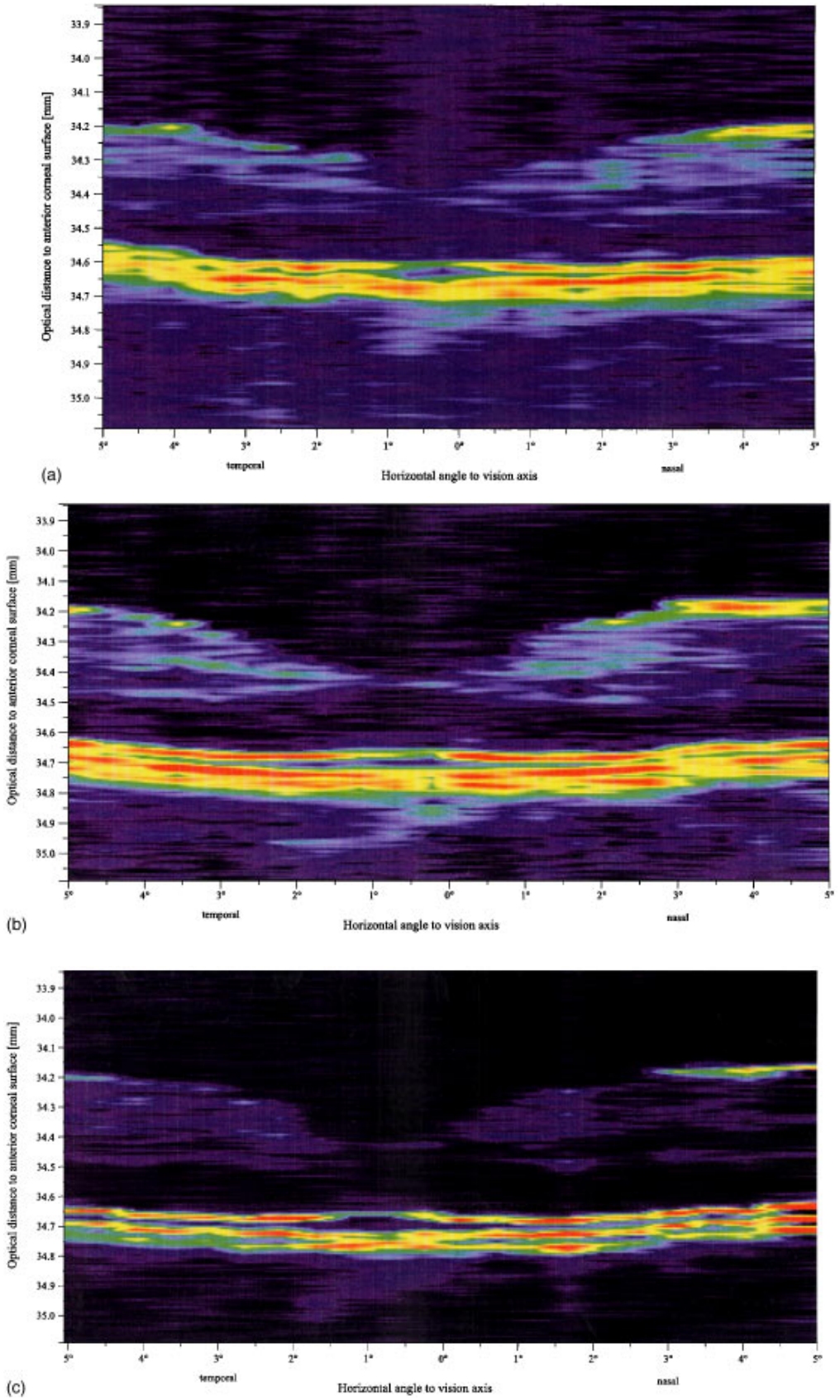

Fig. 6 Retinal tomograms recorded in a human eye *in vivo* demonstrating different longitudinal resolutions, depending on the spectral properties of the light source used. A horizontal section of the fundus across the fovea from 5 deg temporal to 5 deg nasal is shown corresponding to a width of approximately 3 mm on the retina. The vertical scale indicates the optical distance to the anterior corneal surface in millimeters. (a) Single SLD with $\Delta\lambda = 26$ nm without dispersion compensation. (b) Single SLD with $\Delta\lambda = 26$ nm with dispersion compensation. (c) Synthesized light source of two spectrally displaced SLDs with $\Delta\lambda_{eff} = 50$ nm and with dispersion compensation.

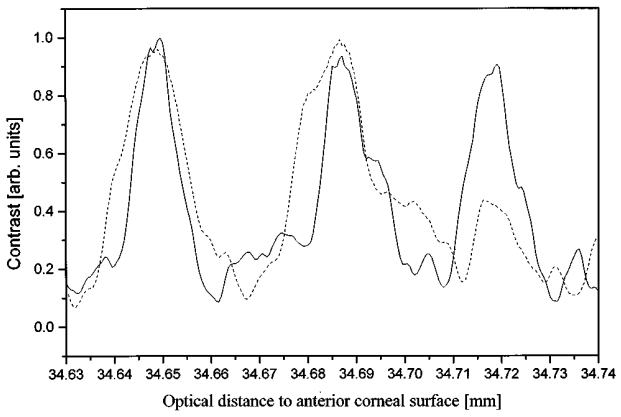

Fig. 7 Optical A-scans recorded with a single SLD without dispersion compensation [dashed line, corresponding to Figure 6(a)], and with the combination source with dispersion compensation [solid line, corresponding to Figure 6(c)] at a measuring angle of 1.5 deg nasal. The improvement in resolution can be clearly observed.

FWHM of the first peak is $\sim$16.5 μm (optical distance) in the case of the dashed curve and $\sim$10 μm in the case of the solid curve. This corresponds to geometrical distances of $\sim$13 and 7 μm, respectively. The second signal peak shows approximately the same factor of improvement. Because the two scans were recorded in different sessions, the overall signal shape is slightly different (it is not possible to maintain exactly the same measuring position on the retina in two successive sessions).

4 DISCUSSION

One of the drawbacks of the dual beam version of PCI and OCT was the poor signal-to-noise ratio. This was caused by the wavefront mismatch of the beams reflected at the retina and the cornea (which is used as a reference surface). Different methods of overcoming this drawback have been suggested: Sekine, Minegishi, and Koizumi developed an axial eye length measurement system based on the tuning of the wavelength of a laser diode. They guided the light to the cornea and the retina through separate optical paths with identical optical path lengths using spatial filtering.[37] Reflections from the cornea and the retina return through their respective paths and interfere with each other after being matched in wavefront shape. The application of this technique for measuring axial eye length in 21 adults *in vivo* has been demonstrated.

Wavefront matching with the use of a special lens with a hole in its optical center was reported by Chen et al.[38] Half of the illuminating beam is focused on the cornea by the special lens, the other part passes through the hole in the center and is focused by the lens of the eye onto the retina. Both of the beams reflected at the cornea and the retina are recollimated by the special lens and the eye lens, respectively, so that all the optical power reflected by the eye may be collected by the photodetector. Hence the intensity of the interfering beams is much higher, yielding a better S/N. By using a single diffractive optical element, we were able to improve the S/N by about 20 to 25 dB in *in vivo* measurements. Compared with the rather complex spatial filtering method used by Chen et al.[38] our solution has the advantage of consisting of a single, lightweight optical element. The lens with the central hole,[38] on the other hand, has the drawback that only a narrow parallel beam can pass through the hole, which restricts the possible resolution on the retina because of the small aperture angle and consequently the rather large diameter of the diffraction-limited probing beam on the retina.

The axial resolution of OCT systems currently used for retinal imaging is claimed to be on the order of 10 to 15 μm.[20–22] Systems with higher resolution using broadband Ti:Al_2O_3 sources have so far been used only for ranging and imaging of tissues with a total thickness of a few hundred micrometers.[23,39] These systems were carefully designed to compensate for the dispersion of the optical elements within the measurement and the reference arm of the interferometer. The additional dispersive effects of a few hundred micrometers of tissue have only a negligible effect on the signal width and hence the resolution. However, if measurements are performed through the relatively thick ocular media to the retina, the dispersive effects of these media have to be compensated for if broadband light sources are used. If a light source with a bandwidth greater than that of a single SLD ($\Delta\lambda\sim$25 nm) is used, the width of the coherence envelope increases and hence the resolution is degraded if the dispersion is not compensated for.[29,30]

We have recently demonstrated a signal width of 5 μm (geometrical distance) in an optical A-scan of a human retina *in vivo* by employing a broadband SLD ($\Delta\lambda\sim$60 nm) with dispersion compensation.[30] Since the output power of this SLD was lower and the spatial coherence of the source was worse than that of usual SLDs, the S/N was rather poor in that case. Therefore we preferred to use a synthesized light source with $\Delta\lambda_{eff}\cong$50 nm generated by superimposing two spectrally displaced SLDs in this work. With this light source and dispersion compensation, we demonstrated the first *in vivo* OCT image of the retina of a human eye with an axial resolution of $\sim$6 to 7 μm (geometrical distance). This is approximately a twofold improvement over existing technology. We were able to resolve structures posterior to the retina that have not been shown by OCT. To identify the histologic origin of these structures, further work has to be done.

We want to point out that the images of Figure 6 were recorded with an experimental laboratory setup in which each scanning angle had to be adjusted manually. Therefore the total scanning time was several minutes and the lateral resolution is

rather poor ($\sim$150 μm). This is not a major drawback of the dual beam PCI technique, but merely a question of the simple scanning device we used in our laboratory work. On the other hand, the images of Figure 6 demonstrate the main advantage of the dual beam technique: its exceptional stability in an axial direction. In spite of the long measuring time, the individual A-scans that were recorded at different angles with time intervals of tens of seconds were mounted on the OCT images without any additional image processing required to correlate the longitudinal positions of the A-scans. This might be helpful in cases where digital postprocessing of the images could lead to loss of fine image details.

5 CONCLUSION

The dual beam partial coherence interferometry technique has been improved by the use of a diffractive optical element for wavefront matching, achieving a significant improvement in the signal-to-noise ratio. To enhance resolution of OCT and PCI for *in vivo* measurements of the posterior structures of the human eye, light sources with broad emission spectra were used together with compensation of the first-order group dispersion of the object to be measured, i.e., the ocular media.

High precision and resolution *in vivo* fundus biometry and imaging were obtained at various positions on the human retina. Hence this improved version of the dual beam PCI is able to obtain localized tomography and biometry of the human eye with high axial resolution.

Acknowledgments

Financial support from the Austrian Science Foundation (FWF grant P 9781-MED) is acknowledged.

REFERENCES

1. R. H. Webb, ''Scanning laser ophthalmoscope,'' in *Noninvasive Diagnostic Techniques in Ophthalmology*, B. R. Masters, ed., pp. 438–450, Springer-Verlag, New York (1990).
2. J. F. Bille, A. W. Dreher, and G. Zinser, ''Scanning laser tomography of the living human eye,'' in *Noninvasive Diagnostic Techniques in Ophthalmology*, B. R. Masters, ed., pp. 528–547, Springer-Verlag, New York (1990).
3. K. Rohrschneider, R. O. W. Burk, F. E. Kruse, and H. E. Völcker, ''Reproducibility of the optic nerve head topography with a new laser tomographic scanning device,'' *Ophthalmology* **101**, 1044–1049 (1994).
4. A. V. Menezes, M. Giunta, L. Chisholm, P. T. Harvey, R. Tuli, and R. G. Devenyi, ''Reproducibility of topographic measurements of the macula with a scanning laser ophthalmoscope,'' *Ophthalmology* **102**(2), 230–235 (1995).
5. A. W. Dreher and K. Reiter, ''Retinal laser ellipsometry: a new method for measuring the retinal nerve fiber layer thickness distribution,'' *Clin. Vis. Sci.* **7**, 481–488 (1992).
6. R. N. Weinreb, S. Shakiba, and L. Zangwill, ''Scanning laser polarimetry to measure the nerve fiber layer of normal and glaucomatous eyes,'' *Am. J. Ophthalmol.* **119**(5), 627–636 (1995).
7. K. Emi, Y. Kobayashi, S. Chujo, C. Fujioka, and M. Yokoyama, ''The biometry of each thickness of the human retina, choroid and sclera by using ultrasound and Fourier analysis—at the foveola,'' *Nippon Ganka Gakki Zasshi* **87**, 74–79 (1983).
8. S. Tane, J. Kohono, J. Horikoshi, K. Kondo, K. Ohashi, A. Komatsu, and T. Kakehashi, ''The study of the microscopic biometry of the thickness of the human retina, choroid, and sclera by ultrasound,'' *Nippon Ganka Gakki Zasshi* **88**, 1412–1417 (1984).
9. R. C. Zeimer, M. T. Mori, and B. Khoobehi, ''Feasibility test of a new method to measure retinal thickness noninvasively,'' *Invest. Ophthal. Vis. Sci.* **30**, 2099–2105 (1989).
10. S. Asrani, R. Zeimer, M. F. Goldberg, and S. Zou, ''Application of rapid scanning retinal thickness analysis in retinal diseases,'' *Ophthalmology* **104**(7), 1145–1151 (1997).
11. A. F. Fercher and E. Roth, ''Ophthalmic laser interferometry,'' *Proc. SPIE* **658**, 48–51 (1986).
12. A. F. Fercher, K. Mengedoht, and W. Werner, ''Eye length measurements by interferometry with partially coherent light,'' *Opt. Lett.* **13**, 186–189 (1988).
13. C. K. Hitzenberger, ''Optical measurement of the axial eye length by laser doppler interferometry,'' *Invest. Ophthalmol. Vis. Sci.* **32**, 616–624 (1991).
14. C. K. Hitzenberger, ''Measurement of corneal thickness by low-coherence interferometry,'' *Appl. Opt.* **31**, 6637–6642 (1992).
15. W. Drexler, A. Baumgartner, O. Findl, C. K. Hitzenberger, H. Sattmann, and A. F. Fercher, ''Submicrometer precision biometry of the anterior segment of the human eye,'' *Invest. Ophthalmol. Vis. Sci.* **38**(7), 1304–1313 (1997).
16. A. Baumgartner, C. K. Hitzenberger, W. Drexler, H. Sattmann, and A. F. Fercher, ''Measurement of the anterior structures of the human eye by partial coherence interferometry,'' *Proc. SPIE* **2330**, 146–151 (1995).
17. W. Drexler, C. K. Hitzenberger, H. Sattmann, and A. F. Fercher, ''Measurement of the thickness of fundus layers by partial coherence tomography,'' *Opt. Eng.* **34**, 701–710 (1995).
18. D. Huang, E. A. Swanson, C. P. Lin, J. S. Schuman, W. G. Stinson, W. Chang, M. R. Hee, T. Flotte, K. Gregory, C. A. Puliafito, and J. G. Fujimoto, ''Optical coherence tomography,'' *Science* **254**, 1178–1181 (1991).
19. A. F. Fercher, C. K. Hitzenberger, W. Drexler, G. Kamp, and H. Sattmann, ''*In vivo* optical coherence tomography,'' *Am. J. Ophthalmol.* **116**, 113–114 (1993).
20. M. R. Hee, J. A. Izatt, E. A. Swanson, D. Huang, J. S. Schuman, C. P. Lin, C. A. Puliafito, and J. G. Fujimoto, ''Optical coherence tomography of the human retina,'' *Arch. Ophthalmol.* **113**(3), 325–332 (1995).
21. C. A. Puliafito, M. R. Hee, C. P. Lin, E. Reichel, J. S. Schuman, J. S. Duker, J. A. Izatt, E. A. Swanson, and J. G. Fujimoto, ''Imaging of macular diseases with optical coherence tomography,'' *Ophthalmology* **102**, 217–229 (1995).
22. A. F. Fercher, ''Optical coherence tomography,'' *J. Biomed. Opt.* **1**(2), 157–173 (1996).
23. B. Bouma, G. J. Tearney, S. A. Boppart, M. R. Hee, M. E. Brezinski, and J. G. Fujimoto, ''High-resolution optical coherence tomographic imaging using a mode-locked Ti:Al_2O_3 laser source,'' *Opt. Lett.* **20**, 1486–1488 (1995).
24. A. G. Podoleanu, G. M. Dobre, D. J. Webb, and D. A. Jackson, ''Coherence imaging by use of a Newton rings sampling function,'' *Opt. Lett.* **21**, 1789–1791 (1996).
25. A. G. Podoleanu, G. M. Dobre, D. J. Webb, and D. A. Jackson, ''Simultaneous en-face imaging of two layers in the Human retina by low-coherence reflectometry,'' *Opt. Lett.* **13**, 1039–1041 (1997).
26. B. Möller, G. Rudolph, A. Klopffleisch, K. H. Donnerhacke, and A. Dorsel, ''Application of diffractive optics for axial eye length measurement using partial coherence interferometry,'' *Proc. SPIE* **2930**, 175–182 (1996).
27. A. Baumgartner, B. Möller, C. K. Hitzenberger, W. Drexler, and A. F. Fercher, ''Measurement of the posterior structures of the human eye *in vivo* by partial coherence interferometry using diffractive optics,'' *Proc. SPIE* **2981**, 85–93 (1997).
28. M. Born and E. Wolf, ''Interference and diffraction with partially coherent light,'' in *Principles of Optics*, pp. 491–555, Pergamon Press, Oxford (1980).
29. C. K. Hitzenberger, W. Drexler, A. Baumgartner, and A. F. Fercher, ''Dispersion effects in partial coherence interferometry,'' *Proc. SPIE* **2981**, 29–36 (1997).

30. C. K. Hitzenberger, A. Baumgartner, W. Drexler, and A. F. Fercher, ''Partial coherence interferometry of the retina with 5 μm resolution by compensation of object dispersion,'' *J. Biomed. Opt.*, submitted for publication.
31. D. N. Wang, Y. N. Ning, K. T. V. Grattan, A. W. Palmer, and K. Weir, ''Optimized multiwavelength combination sources for interferometric use,'' *Appl. Opt.* **33**, 7326–7333 (1994).
32. Y. J. Rao, Y. N. Ning, and D. A. Jackson, ''Synthesized source for white-light sensing systems,'' *Opt. Lett.* **18**, 462–464 (1993).
33. W. Drexler, O. Findl, A. Baumgartner, K. Strenn, G. Rainer, C. K. Hitzenberger, A. F. Fercher, and R. Menapace, ''Dual beam optical coherence tomography and topography of the human eye—a clinical feasibility study,'' *Proc. SPIE* **2930**, 183–193 (1996).
34. W. Drexler, C. K. Hitzenberger, A. Baumgartner, O. Findl, H. Sattmann, and A. F. Fercher, ''Investigation of dispersion effects in ocular media by multiple wavelength partial coherence interferometry,'' Exp. Eye Res., accepted for publication.
35. W. J. Tropf, M. Thomas, and T. J. Harris, ''Properties of crystals and glasses,'' in *Handbook of Optics*, Vol. II, 2nd ed., M. Bass, E. W. Van Stryland, D. R. Williams, and W. L. Wolfe, eds., Chap. 33, McGraw-Hill, New York (1995).
36. American National Standards Institute, *Safe Use of Lasers*, ANSI Z 136.1, American National Standards Institute, New York (1986).
37. A. Sekine, I. Minegishi, and H. Koizumi, ''Axial eye-length measurement by wavelength-shift interferometry,'' *J. Opt. Soc. Am.* **10**, 1651–1655 (1993).
38. S. Chen, D. N. Wang, K. T. V. Grattan, A. W. Palmer, and G. L. Dick, ''A compact optical device for eye-length measurement,'' *IEEE Photonics Technol. Lett.* **5**, 729–731 (1993).
39. X. Clivaz, F. Marquis-Weible, and R. P. Salathé, ''1.5 μm resolution optical low coherence reflectometry in biological tissues,'' *Proc. SPIE* **2083**, 338–346 (1993).